Designing localized waves

By Rod Donnelly[1] and Richard W. Ziolkowski[2]

[1] *Faculty of Engineering and Applied Science, Memorial University, St John's, Newfoundland, Canada A1B 3X5*

[2] *Department of Electrical and Computer Engineering, University of Arizona, Tucson, Arizona 85721, U.S.A.*

In this paper we re-interpret a recently introduced method for obtaining non-separable, localized solutions of homogeneous partial differential equations. This re-interpretation is in the form of a geometrical consideration of the algebraic constraint that the Fourier transforms of such solutions must satisfy in the transform domain (phase space). With this approach we link two classes of localized, non-separable solutions of the homogeneous wave equation, and examine the transform domain characteristic that determines the space-time localization properties of these classes. This characterization allows us to design classes of solutions with better localization properties. In particular, we design and discuss the properties of several novel subluminal and superluminal solutions of the homogeneous wave equation. We also design families of non-separable, localized, subluminal and superluminal solutions of the Klein–Gordon equation by using the same technique.

1. Introduction

In a recent paper (Donnelly & Ziolkowski 1992) we introduced a technique for obtaining interesting solutions of constant coefficient homogeneous partial differential equations. The equation was solved in the Fourier transform domain in essentially an algebraic manner: we manipulated the transform of the candidate for a solution so that it became a generalized function which, when multiplied by the Fourier transform of the differential operator, gave zero in the sense of generalized functions. In particular, we showed how straightforward it was to obtain non-separable 'localized wave' (LW) solutions of the wave equation (Ziolkowski 1985, 1989), the damped wave equation, and the Klein–Gordon equation. These LW solutions propagate with speed c along the z-axis (arbitrarily) and exhibit a degree of localization transverse to the propagation axis (in the ρ variable) that is dependent on an arbitrarily positive parameter. The solutions are particle-like or plane wave-like depending on whether the parameter is large or small, respectively.

In this paper we re-interpret the 'algebraic' method we introduced in a 'geometric' way. This geometric interpretation extends the previous method, and offers a powerful way of designing families of solutions of homogeneous partial differential equations that have desirable localization properties (about the propagation axis).

In §2 we compare two known localized solution families of the homogeneous wave equation (HWE): the fundamental gaussian (focus wave mode) solutions (Ziolkowski 1985, 1989) and the Bessel–Gauss (BG) pulses introduced recently by Overfelt (1991). The Fourier transforms of both solution families share the property that their

Proc. R. Soc. Lond. A (1993) **440**, 541–565
Printed in Great Britain

support lies on the same line. What causes the families to differ is the weighting function associated with this support line. Overfelt demonstrates, in the space-time domain, that the BG pulses have better focusing properties than do the fundamental gaussian pulses, and we demonstrate why this must be so by comparing the weightings associated with the supports of the transform domain representations of both families. This observation allows us to design related families (in the sense of sharing the same support lines) of HWE solutions with even better focusing properties than either the LW or BG pulses.

In §3 we present some new and old solutions of the HWE from this geometrical standpoint. Specifically, we consider the projections of the support lines of the Fourier transforms of HWE solutions onto a plane in the three-dimensional transform space. The projections of the support lines of the transforms of the fundamental gaussian (or BG) pulses, for different values of the arbitrary parameter, span a wedge shaped region of this plane; plane wave HWE solutions are readily seen as limiting cases of these families. Using this concept of projection of the transform domain support line we design particular families of both sub- and superluminal, non-separable, localized HWE solutions (i.e. localized HWE solutions with components travelling less than or greater than speed c, respectively).

The families of non-separable, localized HWE solutions mentioned above all contain (at least) a free parameter, and so a weighted superposition over this parameter will still be a HWE solution. An important consideration is that the weighting, or 'spectrum', of the superposition be chosen so that the total energy of such a superposition is finite. In the case of a superposition of LW pulses, a bound on the spectrum has been derived in order that the superposition have finite total energy (Ziolkowski (1989) and Donnelly & Ziolkowski (1992) give different derivations). In §4 we modify the method derived in the latter reference to obtain an exact expression for the total energy that is applicable to a wide range of HWE solution families. Using this energy expression we investigate bounds on the spectra in the cases of superpositions of the superluminal pulses previously derived, and of the BG pulses introduced by Overfelt (1991) (who did not consider the energy of any associated superpositions).

In §5 we apply the above geometrical method to the Klein–Gordon equation. Rather than catalogue several different solution families, we dwell on two in particular. By choosing the projections of the support lines of the transforms of a particular class of solutions to be a families of straight lines having the same slope in the projection plane, we arrive at families of either superluminal or subluminal non-separable, localized solutions of the Klein–Gordon equation. We comment on the similarity between the Klein–Gordon and HWE localized subluminal pulse solutions: the two solutions provide a link between massless (HWE) and massive (Klein–Gordon equation) localized pulses.

Finally, in §6 we discuss the merits of the work presented, and suggest avenues for further investigation.

2. Known localized solutions of the HWE

In a recent paper (Donnelly & Ziolkowski 1992) we introduced a technique for obtaining interesting solutions of constant constant coefficient homogeneous linear partial differential equations. In particular, we obtained the non-separable LW solutions of the wave equation (Ziolkowski 1985, 1989), the damped wave equation,

and the Klein–Gordon equation. These solutions propagate with speed c along the z axis (arbitrarily) and exhibit a degree of localization transverse to the propagation axis (the ρ axis) that is dependent on an arbitrary positive parameter.

As in our previous paper, here we shall address most of our detailed remarks to the free space homogeneous wave equation (HWE),

$$\left(\nabla^2 - \frac{1}{c^2}\frac{\partial^2}{\partial t^2}\right)\psi(\boldsymbol{r}, t) = 0; \tag{1}$$

the analysis here is readily extended to other homogeneous partial differential equations in subsequent sections. We introduce the multidimensional Fourier transform pair

$$\left.\begin{aligned} \Psi(\boldsymbol{k}, \omega) \equiv \mathscr{F}_{r,t}\{\psi\}(\boldsymbol{k}, \omega) \equiv \mathscr{F}_{r}\mathscr{F}_{t}\{\psi\}(\boldsymbol{k}, \omega) = \int_{\mathbb{R}^3} \mathrm{d}\boldsymbol{r} \int_{-\infty}^{\infty} \mathrm{d}t\, \psi(\boldsymbol{r}, t)\, \mathrm{e}^{-\mathrm{i}\boldsymbol{k}\cdot\boldsymbol{r}} \mathrm{e}^{\mathrm{i}\omega t}, \\ \psi(\boldsymbol{r}, t) = \frac{1}{(2\pi)^4} \int_{\mathbb{R}^3} \mathrm{d}\boldsymbol{k} \int_{-\infty}^{\infty} \mathrm{d}\omega\, \Psi(\boldsymbol{k}, \omega)\, \mathrm{e}^{\mathrm{i}\boldsymbol{k}\cdot\boldsymbol{r}} \mathrm{e}^{-\mathrm{i}\omega t}. \end{aligned}\right\} \tag{2}$$

In (2) we denote the vector whose cartesian components are (k_x, k_y, k_z), the spatial transform variables, by $\boldsymbol{k}$, and ω is the temporal transform variable. Taking the Fourier transform of (1) gives

$$(k^2 - \omega^2/c^2)\, \mathscr{F}_{r,t}\{\psi\}(\boldsymbol{k}, \omega) = 0. \tag{3}$$

In the sense of generalized functions, we have the result

$$f(\boldsymbol{v})\, \delta(\boldsymbol{v} - \boldsymbol{v}_0) = f(\boldsymbol{v}_0)\, \delta(\boldsymbol{v} - \boldsymbol{v}_0), \tag{4}$$

for a suitably well-behaved function f, where $\boldsymbol{v}$ is an n-dimensional vector variable, $\boldsymbol{v}_0$ a constant vector, and δ denotes the n-dimensional delta function. With the use of (4) we showed how to construct readily solutions ψ of (1) which represent weighted superpositions of either plane waves or spherical waves. If we rewrite (3)

$$(\kappa^2 + k_z^2 - \omega^2/c^2)\, \mathscr{F}_{r,t}\{\psi\}(\boldsymbol{k}, \omega) = 0, \tag{5}$$

where $\kappa^2 = k_x^2 + k_y^2$, then it is straightforward to verify that any solution of the form

$$\Xi(\kappa, \beta)\, \delta[k_z - (\beta - \kappa^2/4\beta)]\, \delta[\omega + c(\beta + \kappa^2/4\beta)], \tag{6}$$

where the weighting Ξ is an arbitrary function, will satisfy (5). This is because the delta functions in (6) will constrain the term $\kappa^2 + k_z^2 - \omega^2/c^2$ to be identically zero.

The choice of weighting

$$\Xi(\kappa, \beta) = (\pi^2/\mathrm{i}\beta) \exp(-\kappa^2 z_0/4\beta), \tag{7}$$

where we assume that $\beta > 0$ and $z_0 > 0$ are arbitrary, leads to the *focus wave mode* (FWM) solution (Ziolkowski 1985, 1989) of (1):

$$\psi_{\mathrm{FWM}}(\boldsymbol{r}, t; \beta) = \mathrm{e}^{\mathrm{i}\beta(z+ct)} \frac{\exp(-\rho^2\beta/[z_0 + \mathrm{i}(z - ct)])}{4\pi\mathrm{i}[z_0 + \mathrm{i}(z - ct)]}. \tag{8}$$

Any weighted superposition over the parameter β, for example,

$$\int_0^{\infty} \mathrm{d}\beta\, F(\beta)\, \psi_{\mathrm{FWM}}(\boldsymbol{r}, t; \beta), \tag{9}$$

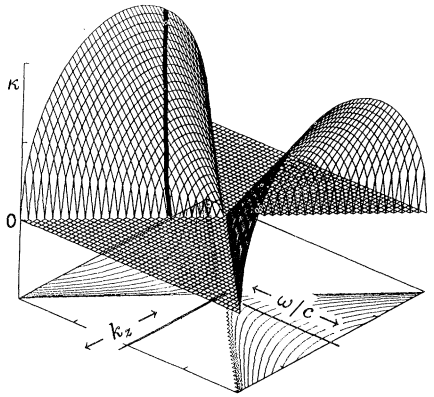

Figure 1. Support line of the transform domain function given in (6). The support line, which is shown lying on a portion of the surface $\kappa^2+k_z^2-(\omega/c)^2=0$, is described by the two equations in (12).

will also be a localized HWE solution. The superposition (9) can be shown (Ziolkowski 1989; Donnelly & Ziolkowski 1992) to have finite energy provided

$$\int_0^\infty \mathrm{d}\beta \frac{|F(\beta)|^2}{\beta} < \infty. \tag{10}$$

The key to understanding the non-separability and the localized natures of the FWM solutions (8) is to examine, respectively, the delta function constraints and the weighting term, Ξ, in the transform domain representation, (6).

The two delta functions in (6) have the effect of forcing any function of the transform domain variables κ, k_z, and ω to lie on the surface

$$\kappa^2+k_z^2-(\omega/c)^2=0. \tag{11}$$

In particular, the support of the delta functions is the line described by the two equations

$$k_z=\beta-\kappa^2/4\beta, \quad \omega/c=-(\beta+\kappa^2/4\beta). \tag{12}$$

This line is shown on the surface (11) in figure 1. We realize that any solution of (5) can be considered as a generalized function which, when multiplied by $\kappa^2+k_z^2-(\omega/c)^2$, equals zero in the sense of generalized functions. As such, the support of any solution of (5) will lie on the surface (11).

It is convenient to consider the projection of the support of the solutions of (5) onto the k_z, ω/c plane. The projection of the support curve of the FWM solution, given in (12), is shown in figure 2 for arbitrary β. It consists of a straight line, of slope one, ending at the point (β,β). When $\beta=0$ the projection of the 'solution line' on the surface (11) coincides with the solution line itself; it is the line given by $\omega/c=k_z$, $\kappa=0$, and corresponds to a superposition of plane waves, each with frequency ω and speed c, travelling in the positive z direction. This gives a 'geometric' justification for the 'algebraic' notion implied previously by us, that the FWM solutions represent the next generalization of HWE solutions from plane waves: in the transform domain the FWM solutions represent a parallel translation of the straight support line from the k_z, ω/c plane onto the elevated surface given in (11) and shown in figure 1.

The particular form (8) of the LW solutions is due not only to the support line,

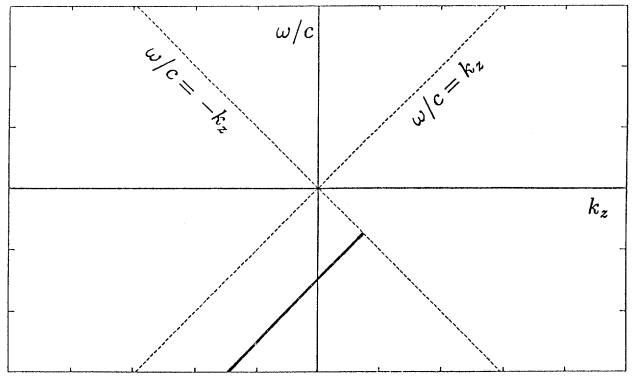

Figure 2. Projection of the support line of the transform of the HWE solution, given in (12) and shown in figure 1, onto the k_z, ω/c plane.

described by (12), on the surface (11), but also to the choice of the weighting function along the support line. Clearly, there are many possible weightings leading to other LW solutions. As another example, consider

$$\Xi(\kappa,\lambda,\beta) = (z_0 4\pi^3/\beta) I_0(\lambda z_0 \kappa/2\beta) \exp(-\lambda^2 z_0/4\beta) \exp(-z_0\kappa^2/4\beta), \tag{13}$$

where $z_0 > 0$, $\beta > 0$, and $\lambda > 0$ are arbitrary parameters. In fact, this choice of weighting in (6) can be shown to lead to the so-called zero-order 'Bessel–Gauss' (BG) pulse, introduced recently by Overfelt (1991):

$$\psi_{\mathrm{BG},0}(\boldsymbol{r},t) = \frac{z_0}{z_0+\mathrm{i}(z-ct)} J_0\left(\frac{\lambda z_0 \rho}{z_0+\mathrm{i}(z-ct)}\right) \exp[\mathrm{i}\beta(z+ct)]$$
$$\times \exp[-\beta\rho^2/[z_0+\mathrm{i}(z-ct)]] \exp[-\mathrm{i}\lambda^2 z_0(z-ct)/4\beta[z_0+\mathrm{i}(z-ct)]]. \tag{14}$$

As pointed out by Overfelt (1991), taking the limit $\lim_{\lambda\to 0} \psi_{\mathrm{BG},0}(\boldsymbol{r},t)$ leaves us with the LW pulse, (8), with parameter β. One can show that the general nth-order BG pulse again has a Fourier transform as given by (6), but this time with the weighting function

$$\Xi_{\mathrm{BG},n}(\kappa,\lambda,\beta) = (z_0 4\pi^3 \mathrm{e}^{\pm \mathrm{i}n(\pi/2+\varphi)}/\beta) I_n(\lambda z_0 \kappa/2\beta) \exp(-\lambda^2 z_0/4\beta) \exp(-z_0\kappa^2/4\beta), \tag{15}$$

where φ is the angular variable in a conventional cylindrical $[\kappa,\varphi,k_z]$ decomposition of $\boldsymbol{k}$-space. As stated by Overfelt, the zero-order BG pulse can be shown to be 'more highly localized' than the fundamental FWM of Ziolkowski, 'because of its extra spectral degree of freedom', as evidenced by the arbitrary parameter λ in (13).

For any HWE solution whose transform domain representation is of the form (6), the degree of localization in the ρ direction (perpendicular to the z propagation axis) is determined by the choice of weighting function of κ, Ξ. One can demonstrate the following inequality with standard Fourier transform results:

$$(W\times B) \equiv \frac{\int_{\mathbb{R}^2} \mathrm{d}x\,\mathrm{d}y\,\rho^2 |\psi(\rho,z,t)|^2}{\int_{\mathbb{R}^2} \mathrm{d}x\,\mathrm{d}y\,|\psi(\rho,z,t)|^2} \times \frac{\int_{\mathbb{R}^2} \mathrm{d}k_x\,\mathrm{d}k_y\,\kappa^2 |\mathscr{F}_{x,y}\{\psi\}(\kappa,z,t)|^2}{\int_{\mathbb{R}^2} \mathrm{d}k_x\,\mathrm{d}k_y |\mathscr{F}_{x,y}\{\psi\}(\kappa,z,t)|^2} \geqslant \frac{1}{2}. \tag{16}$$

The inequality (16) corresponds to the so-called 'uncertainty relation', in communications, for the duration-bandwidth product of time signals. The first

quotient on the left in (16) can be interpreted as a 'waist' of the HWE solution about the z-axis, with the second as a 'spatial bandwidth' of the solution with respect to the transverse distance transform variable.

If we compare the weighting functions Ξ for the FWM and BG pulses, given respectively in (7) and (13), we see that the BG pulses have an extra term $I_0(\lambda z_0 \kappa/2\beta)$ included. The decay of the transform domain representation (on the line of support of the two delta functions in (6)) of the BG pulse due to the $\exp(-z_0\kappa^2/4\beta)$ term will be tempered by the modified Bessel function, which behaves asymptotically like $\exp(\lambda z_0\kappa/2\beta)/\sqrt{(2\pi\lambda z_0\kappa/2\beta)}$. One would thus intuitively expect that the second, bandwidth, term on the left side of (16) would be greater for the BG pulses than for the FWM pulses; indeed, this effect should be evident the larger λ becomes. But, in order that the inequality in (16) be satisfied, this is exactly the effect we should expect to see if we were to 'pinch' our FWM solution (i.e. decrease its waist): a corresponding increase in its spatial bandwidth. These intuitive notions are made more exact in Appendix A.

3. New and old solutions of the HWE

As mentioned in §2, both the FWM and BG pulses are similar in that their temporal and spatial Fourier transform domain representations consist of lines (the support of the product of delta functions in (6)) lying on the surface $\kappa^2+k_z^2-(\omega/c)^2=0$, as shown in figure 1. They differ in the weighting (Ξ in (6)) along this line. It is easy to see that every rotationally invariant (with respect to the z propagation axis) solution of the HWE corresponds to some subset of this surface (whether it be a point, line, or patch, for example), accompanied by a suitable weighting. Actually, even more general LW solutions (varying with ϕ in a (ρ, ϕ, z) spatial cylindrical coordinate system) may be accommodated in this way, if along with the transform domain weighting we include a function of φ, where we have decomposed the spatial transform domain into a conventional (κ, φ, k_z) cylindrical coordinate system. Furthermore, because of the obvious bijection, to consider HWE solution subsets of the surface $\kappa^2+k_z^2-(\omega/c)^2=0$, it suffices to consider their projection on to the k_z, ω/c plane. We shall now consider examples of projections of various HWE solution lines, some possible weightings, and the localized HWE solutions to which they correspond.

(a) *Plane waves*

As discussed previously (Donnelly & Ziolkowski 1992), the choice of the transform domain solution

$$\mathscr{F}_{r,t}\{\psi\}(\kappa, k_z, \omega) = \beta(\omega)\,(\delta(\kappa)/\kappa)\,\delta(k_z \pm \omega/c) \tag{17}$$

corresponds in space-time to a superposition (over ω) of plane waves travelling in the negative/positive z direction. In this case the solution line in (17) is either 'edge' of the surface $\kappa^2+k_z^2-(\omega/c)^2=0$; the projection of the line is itself. As $\kappa=0$ on this solution line, the weighting function, β, is a function of the single (arbitrary) parameter ω; this lack of variation with κ on the solution line also leads to separability of the solution.

(b) *Focus wave mode (FWM) or Bessel–Gauss (BG) pulses*

We reproduce here the transform domain solution (6), for convenience:

$$\mathscr{F}_{r,t}\{\psi\}(\kappa, k_z, \omega) = \Xi(\kappa, \beta, \lambda)\,\delta[k_z-(\beta-\kappa^2/4\beta)]\,\delta[\omega+c(\beta+\kappa^2/4\beta)], \quad \beta>0. \tag{18}$$

The projection of the solution line corresponding to (18) is the straight line, of slope $+1$ (with respect to k_z), given by that portion of

$$(\omega/c) = k_z - 2\beta \tag{19}$$

for which $\omega < -2\beta$. In figure 2 we have shown the projection of the solution line (that portion of (19)) for two values of β: β_1 and $\beta_2 > \beta_1$, along with the contour lines of the surface $\kappa^2 + k_z^2 - (\omega/c)^2 = 0$. With this representation of solutions of the form (18), several properties are apparent. Both the FWM and BG pulses have cut-offs in their temporal and z spatial spectra: the spectra are zero for $\omega/c > -\beta$ and $k_z > +\beta$. The result $\mathscr{F}_t\{\psi\}(\omega) = (\mathscr{F}_t(\psi^*\}(-\omega))^*$ implies that the temporal Fourier transform of the real part of any HWE solution of the form (18) will be zero in the range $-c\beta < \omega < c\beta$ (mentioned in Donnelly & Ziolkowski (1992)). As β is increased, the projection of the HWE solution line crosses contour lines at a greater rate. However, in the case of both the FWM and BG pulses, whose transform domain representations contain the factor $\exp(-\kappa^2 z_0/4\beta)$, as β is increased we see that the weighting decreases more slowly as κ increases. Thus one would expect a greater spatial bandwidth, B, as defined through (16). We know that, as β increases, both the FWM and BG pulses become more highly localized (their waists decrease), and so we expect an accompanying increase of spectral bandwidth. As $\beta \to 0$ the projection line tends to that of plane waves, given in example (1), and the weighting tends to one.

(*c*) *Other* LW *pulses having speed c*

The projections of the solution lines corresponding to the delta function constraint in (18) (for $\beta > 0$ varying) forms but one general family of projections of HWE solution lines: $\beta > 0$, $\omega < 0$, slope $+1$. There are clearly three other related families: $\beta > 0$, $\omega < 0$, slope -1 (corresponding to HWE solutions that propagate in the negative z direction with speed c), $\beta < 0$, $\omega > 0$, slope $+1$ (solutions propagate in the positive z direction with speed c), and $\beta < 0$, $\omega < 0$, slope -1 (solutions propagate in the negative z direction with speed c). Just as in the case of FWM or BG pulses, one may form new localized HWE solutions from these alternate families by superposing weighted solutions with respect to the parameter β.

(*d*) *Superluminal pulses: varying speed projections*

In figure 3 we have shown an arbitrary straight line emanating from the origin in the $k_z, \omega/c$ plane, lying in the upper half-plane between the lines $\omega/c = \pm k_z$. We take this line to be the projection line of a typical member of a new family of HWE solution lines, again lying on the surface $\kappa^2 + k_z^2 - (\omega/c)^2 = 0$. With γ any real number lying in the range $(-1, 1)$, we see that on the projection line shown $k_z/(\omega/c) = \gamma$, and $\omega/c > 0$ (i.e. γ is the reciprocal slope).

From this characterization of the projection line it is straightforward to determine the corresponding HWE solution line. This solution line will, in turn, correspond to the HWE solution whose Fourier transform is given by

$$\mathscr{F}_{r,t}\{\psi_\gamma\}(\kappa, k_z, \omega) = \Xi(\kappa, \gamma)\,\delta(k_z - \gamma\kappa/\sqrt{(1-\gamma^2)})\,\delta(\omega - c\kappa/\sqrt{(1-\gamma^2)}), \tag{20}$$

where, again, $\Xi(\kappa, \gamma)$ is an arbitrary weighting function to be associated with the solution line.

If we now choose as weighting

$$\Xi(\kappa, \gamma) = \frac{(2\pi)^3\gamma^2}{(1-\gamma^2)} \exp[-z_0|\gamma|\,\kappa/\sqrt{(1-\gamma^2)}], \tag{21}$$

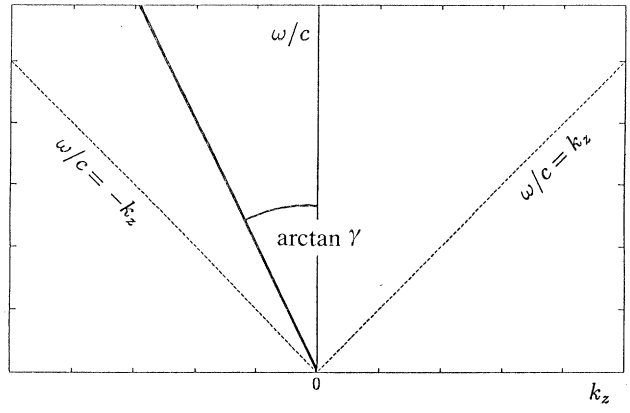

Figure 3. Projection of the support line of the transform of the superluminal HWE solution, given through (20), onto the k_z, ω/c plane.

Figure 4

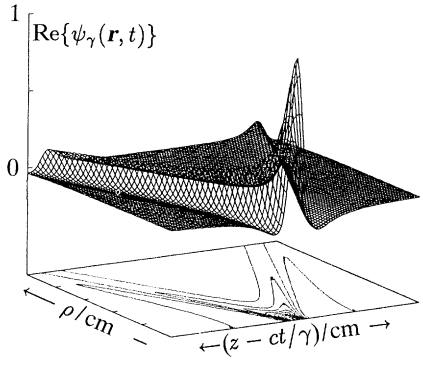

Figure 5

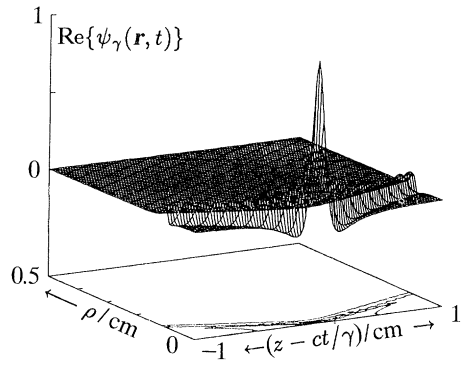

Figure 4. Normalized surface plot of the superluminal HWE solution pulse $\mathrm{Re}\{\psi_\gamma(\boldsymbol{r},t)\}$, where ψ_γ is given in (23), for the values $t=0$, $z_0=0.1$, $|z-ct/\gamma|\leqslant 1$ cm, $0\leqslant\rho\leqslant 0.5$ cm, and $\gamma=0.5$. The pulse centre travels with speed $2c$.

Figure 5. Normalized surface plot of the superluminal HWE solution pulse $\mathrm{Re}\{\psi_\gamma(\boldsymbol{r},t)\}$, where ψ_γ is given in (23), for the values $t=0$, $z_0=0.1$, $|z-ct/\gamma|\leqslant 1$ cm, $0\leqslant\rho\leqslant 0.5$ cm, and $\gamma=1.0$. The pulse centre now travels with speed $10c$. Note that the leading and trailing 'Mach cones' have correspondingly smaller vertex angles as compared with the $2c$ pulse in figure 4.

where $z_0>0$ is arbitrary, the exact space-time form of the HWE solution given through (20) may be determined. Applying inverse spatial and temporal Fourier transforms to (20) gives, eventually,

$$\psi_\gamma(\boldsymbol{r},t)=\frac{\gamma^2}{(1-\gamma^2)}\int_0^\infty \mathrm{d}\kappa\,\kappa J_0(\kappa\rho)\exp\left\{-\frac{\kappa[z_0|\gamma|-\mathrm{i}\gamma(z-ct/\gamma)]}{\sqrt{(1-\gamma^2)}}\right\}. \tag{22}$$

This integral may be evaluated (Gradshteyn & Ryzhik 1980, eq. 6.623.2) to give

$$\psi_\gamma(\boldsymbol{r},t)=\frac{[z_0-\mathrm{i}\,\mathrm{sgn}\,(\gamma)\,(z-ct/\gamma)]}{\{\rho^2((1-\gamma^2)/\gamma^2)+[z_0-\mathrm{i}\,\mathrm{sgn}\,(\gamma)\,(z-ct/\gamma)]^2\}^{\frac{3}{2}}}. \tag{23}$$

As $-1<\gamma<1$, we realize that ψ_γ in (23) represents a waveform that is travelling in the positive/negative z direction, depending on whether γ is positive/negative, with speed $|c/\gamma|>1$. That is, ψ_γ in (23) is a superluminal pulse whose speed depends on

γ. From (23) we also see that at the pulse centre $z = ct/\gamma$, the superluminal pulse decays like $1/\rho^3$. This is to be compared with the co-called 'sling-shot' superluminal LW HWE solution found by Ziolkowski *et al.* (1993), which has a weaker decay of only $1/\rho$. In figures 4 and 5 we have shown surface plots of the superluminal HWE solution pulse $\mathrm{Re}\{\psi_\gamma(\boldsymbol{r}, t)\}$, for ψ_γ as given in (23), for two different values of γ (corresponding, respectively, to pulse centre speeds of $2c$ and $10c$). Note that the leading and trailing 'Mach cones' have smaller vertex angles for the faster pulse.

(*e*) *Superluminal pulses: constant speed projections*

In figure 6 we have shown three arbitrary straight lines, each having the same reciprocal slope $\gamma_0 (0 < \gamma_0 < 1)$, all emanating from the line $\omega/c = -k_z, \omega/c > 0$. These three lines are projections of members of a family of HWE solution lines; an arbitrary projection line may be written as

$$k_z = \gamma_0[(\omega/c) - \beta], \quad \omega/c > \gamma_0\beta/(1+\gamma_0), \tag{24}$$

where $\beta \geqslant 0$ is arbitrary. From this characterization of the projection we may readily determine the corresponding HWE solution line. This solution line will, in turn, correspond to a HWE solution whose Fourier transform is given by

$$\begin{aligned}\mathscr{F}_{r,t}\{\psi_{\gamma_0,\beta}\}(\kappa, k_z, \omega) = \Xi(\kappa, \gamma_0, \beta)\, \delta(k_z - \gamma_0[-\beta + \sqrt{[\kappa^2(1-\gamma_0^2) + \gamma_0^2\beta^2]}]/(1-\gamma_0^2)) \\ \times \delta(\omega - c[-\beta\gamma_0^2 + \sqrt{[\kappa^2(1-\gamma_0^2) + \gamma_0^2\beta^2]}]/(1-\gamma_0^2)),\end{aligned} \tag{25}$$

where, again, $\Xi(\kappa, \gamma_0, \beta)$ is an arbitrary weighting function to be associated with the solution line. If we now choose

$$\Xi(\kappa, \gamma_0, \beta) = \frac{(2\pi)^3}{\kappa\sqrt{(\kappa^2 + \nu_0^2)}} \exp(-z_0\gamma_0\sqrt{(\kappa^2 + \nu_0^2)}/\sqrt{(1-\gamma_0^2)}), \tag{26}$$

where $\nu_0^2 = \gamma_0^2\beta^2/(1-\gamma_0^2)$, the exact space-time form of the HWE solution given through (25) may be determined. Applying inverse spatial and temporal Fourier transforms to (25) gives, eventually,

$$\psi_{\gamma_0,\beta}(\boldsymbol{r}, t) = \exp\left(-\frac{\mathrm{i}\beta\gamma_0[z - \gamma_0 ct]}{(1-\gamma_0^2)}\right) \int_0^\infty \mathrm{d}\kappa \frac{J_0(\kappa\rho)}{\sqrt{(\kappa^2 + \nu_0^2)}} \exp(-\chi\sqrt{(\kappa^2 + \nu_0^2)}), \tag{27}$$

where we use χ defined by

$$\chi = \frac{\gamma_0}{\sqrt{(1-\gamma_0^2)}}[z_0 - \mathrm{i}(z - ct/\gamma_0)]. \tag{28}$$

The integral in (27) may be evaluated (Gradshteyn & Ryzhik 1980, eq. 6.637.1) to give

$$\begin{aligned}\psi_{\gamma_0,\beta}(\boldsymbol{r}, t) = \exp(-\mathrm{i}\beta\gamma_0[z - \gamma_0 ct]/(1-\gamma_0^2)) \\ \times I_0\left\{\frac{\beta\gamma_0^2}{1-\gamma_0^2}\left[\sqrt{\left\{\left[z_0 - \mathrm{i}\left(z - \frac{ct}{\gamma_0}\right)\right]^2 + \frac{\rho^2(1-\gamma_0^2)}{\gamma_0^2}\right\}} - \left[z_0 - \mathrm{i}\left(z - \frac{ct}{\gamma_0}\right)\right]\right]\right\} \\ \times K_0\left\{\frac{\beta\gamma_0^2}{1-\gamma_0^2}\left[\sqrt{\left\{\left[z_0 - \mathrm{i}\left(z - \frac{ct}{\gamma_0}\right)\right]^2 + \frac{\rho^2(1-\gamma_0^2)}{\gamma_0^2}\right\}} + \left[z_0 - \mathrm{i}\left(z - \frac{ct}{\gamma_0}\right)\right]\right]\right\},\end{aligned} \tag{29}$$

where I_0 and K_0 are the usual modified Bessel functions. Again, since $0 \leqslant \gamma_0 < 1$, $\psi_{\gamma_0,\beta}$ in (29), this HWE solution represents a waveform whose envelope is travelling in the positive z direction, with speed $c/\gamma_0 > 1$; i.e. a superluminal pulse.

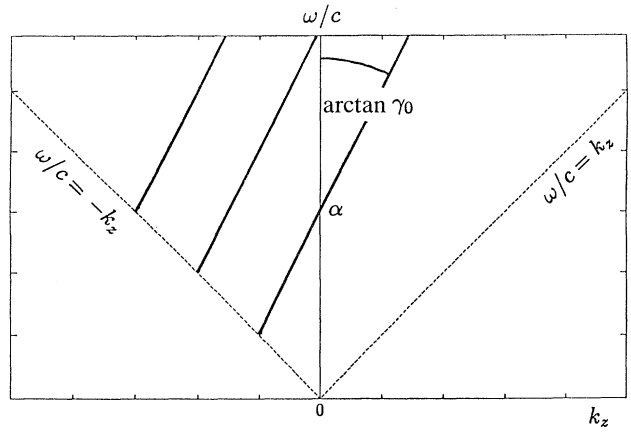

Figure 6. Projection of the support lines of the transforms of three members of a constant speed superluminal family of HWE solutions, given through (24), for three arbitrary values of β.

Figure 7

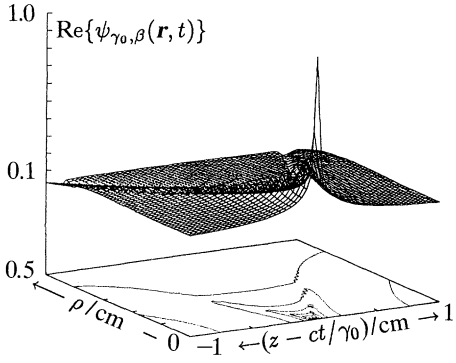

Figure 8

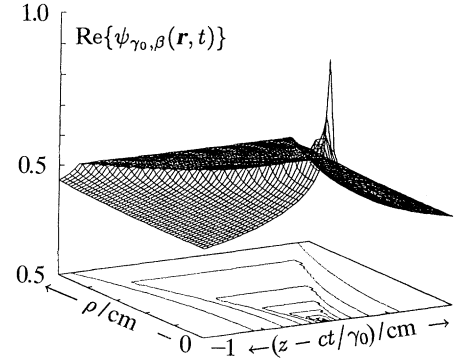

Figure 7. Normalized surface plot of the superluminal HWE solution pulse $\mathrm{Re}\{\psi_{\gamma_0,\beta}(\boldsymbol{r},t)\}$, where $\psi_{\gamma_0,\beta}$ is given in (29), for the values $t=0$, $z_0=0.001$, $\beta=10$, $|z-ct/\gamma_0|\leqslant 1$ cm, $0\leqslant\rho\leqslant 0.5$ cm and $\gamma_0=0.5$. The pulse centre travels with speed $2c$.

Figure 8. Normalized surface plot of the superluminal HWE solution pulse $\mathrm{Re}\{\psi_{\gamma_0,\beta}(\boldsymbol{r},t)\}$, where $\psi_{\gamma_0,\beta}$ is given in (29), for the values $t=0$, $z_0=0.001$, $\beta=0.01$, $|z-ct/\gamma_0|\leqslant 1$ cm, $0\leqslant\rho\leqslant 0.5$ cm and $\gamma_0=0.5$. The pulse centre travels with speed $2c$. Note the broadening of the pulse waist, as compared with figure 7.

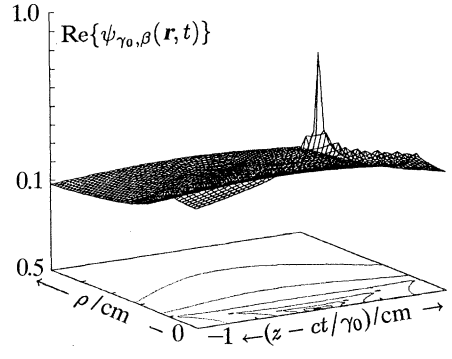

Figure 9. Normalized surface plot of the superluminal HWE solution pulse $\mathrm{Re}\{\psi_{\gamma_0,\beta}(\boldsymbol{r},t)\}$, where $\psi_{\gamma_0,\beta}$ is given in (29), for the values $t=0$, $z_0=0.001$, $\beta=10$, $|z-ct/\gamma_0|\leqslant 1$ cm, $0\leqslant\rho\leqslant 0.5$ cm and $\gamma_0=0.1$. The pulse centre travels with speed $10c$. Note that the leading and trailing 'Mach cones' have correspondingly smaller vertex angles than have the $2c$ superluminal pulse in figure 7.

As complicated as the expression for $\psi_{\gamma_0,\beta}$ is, in (29), it represents a HWE solution exhibiting a certain degree of localization, with respect to the propagation axis. Indeed, for $z = ct/\gamma_0$, and $\rho \gg 0$, we can make use of the first term in the asymptotic expansions for I_0 (given in (A5)) and for K_0, given by (Abramowitz & Stegun 1965, eq. 9.7.2)

$$K_0(\zeta) \sim \sqrt{(\pi/2\zeta)}\,\mathrm{e}^{-\zeta}, \tag{30}$$

to approximate

$$|\psi_{\gamma_0,\beta}(\rho \gg 0, z = ct/\gamma_0, t)| \approx \frac{\sqrt{(1-\gamma_0^2)}\exp[-2z_0\beta\gamma_0^2/(1-\gamma_0^2)]}{2\beta^2\gamma_0\sqrt{[\rho^2 - z_0^2\gamma_0^2/(1-\gamma_0^2)]}}, \tag{31}$$

where we neglect all terms of order $1/\rho$ in the arguments of the modified Bessel functions. Thus, the superluminal pulse given in (29) decays like $1/\rho$ for large ρ. Note also that the 'far field' (in (31)), is exponentially smaller for those HWE solutions, in this family, that correspond to larger β values.

In figures 7–9 we have shown normalized surface plots of the superluminal HWE solution pulse $\mathrm{Re}\{\psi_{\gamma_0,\beta}(\boldsymbol{r}, t)\}$, where $\psi_{\gamma_0,\beta}$ given in (29), for different values of β and γ_0. It is seen that decreasing β causes the pulse to broaden, while decreasing γ_0 (speeding the pulse up) causes a corresponding decrease in the vertex angles of the leading and trailing 'Mach cones'.

(*f*) *Subluminal pulse*: *constant speed projections*

In figure 10 we have shown two arbitrary straight lines, each having the same reciprocal slope $\gamma_0 > 1$, both running between the lines $\omega/c = \pm k_z$ in the upper half-plane $\omega/c > 0$, and each cutting the ω/c axis at different values, β_1, and β_2.

These lines are projections of members of a family of HWE solution lines. An arbitrary projection line may be written as that portion of the straight line

$$k_z = \gamma_0[(\omega/c) - \beta] \tag{32}$$

lying between the lines $\omega/c = \pm k_z$. We realise that, on the corresponding HWE solution line, κ will vary from zero up to some maximum value (depending on γ_0 and β) and then back to zero. It is not difficult to show that the peak value of κ (given by $\beta\gamma_0/\sqrt{(\gamma_0^2-1)}$) on any HWE solution line occurs for those values of ω/c and k_z where the corresponding projection line intersects the straight line $\omega/c = \gamma_0 k_z$. There will be two points on any HWE solution line with the same value of κ in the range $0 < \kappa < \beta\gamma_0/\sqrt{(\gamma_0^2-1)}$. This is to be compared with the luminal and superluminal cases, where for each HWE solution line there was a bijection onto κ values in the range $[0, \infty)$. Thus, here the HWE solution line breaks down naturally into two segments, as does the corresponding projection line (where the straight line segments will be of equal length). We may associate different weightings with each segment of the solution line. The general form of the Fourier transform of the HWE solution whose projection line is shown in figure 10 is given by

$$\begin{aligned}\mathscr{F}_{r,t}\{\psi_{\gamma_0,\beta}\}(\kappa, k_z, \omega) = {} & \Xi_1(\kappa, \gamma_0, \beta)\,\delta(k_z - \gamma_0[\beta + \sqrt{[\beta^2\gamma_0^2 - \kappa^2(\gamma_0^2-1)]}]/(\gamma_0^2-1)) \\ & \times \delta(\omega - c[\beta\gamma_0^2 + \sqrt{[\gamma_0^2\beta^2 - \kappa^2(\gamma_0^2-1)]}]/(\gamma_0^2-1)) \\ & + \Xi_2(\kappa, \gamma_0, \beta)\,\delta(k_z - \gamma_0[\beta - \sqrt{[\beta^2\gamma_0^2 - \kappa^2(\gamma_0^2-1)]}]/(\gamma_0^2-1)) \\ & \times \delta(\omega - c[\beta\gamma_0^2 - \sqrt{[\beta^2\gamma_0^2 - \kappa^2(\gamma_0^2-1)]}]/(\gamma_0^2-1)),\end{aligned} \tag{33}$$

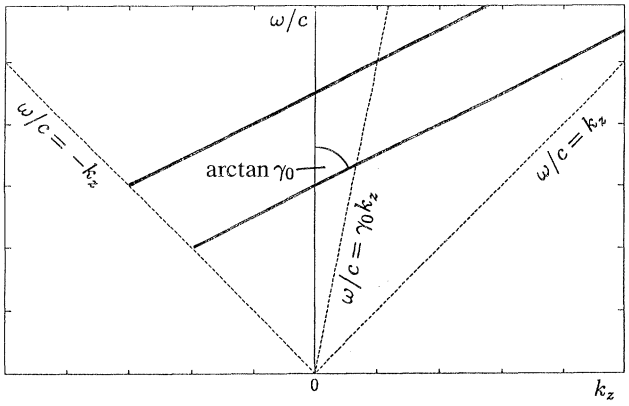

Figure 10. Projection of the support lines of the transforms of two members of a constant speed subluminal family of HWE solutions, given through (32), for two arbitrary β values. For the corresponding support lines, the maximum value of κ will occur where the support line projection intersects the line $\omega/c = \gamma_0 k_z$ (shown).

for κ in the range $0 \leqslant \kappa \leqslant \beta\gamma_0/\sqrt{(\gamma_0^2-1)} \equiv \kappa_0$, where Ξ_1 and Ξ_2 are arbitrary weighting functions. If we now choose

$$\Xi_1(\kappa, \gamma_0, \beta) \equiv \Xi_2(\kappa, \gamma_0, \beta) = (2\pi)^3/2\sqrt{(\kappa_0^2-\kappa^2)}, \tag{34}$$

then the exact space-time form of the HWE solution defined by (33) may be determined. Applying inverse spatial and temporal Fourier transforms to (33) gives, eventually,

$$\psi_{\gamma_0,\beta}(\rho, z, t) = \kappa_0 \exp\left(\frac{\mathrm{i}\beta\gamma_0[z-\gamma_0 ct]}{(\gamma_0^2-1)}\right)\int_0^\infty \mathrm{d}\xi \frac{\xi J_0(\kappa_0\rho\xi)}{\sqrt{(1-\xi^2)}} \times \cos\left\{\frac{\gamma_0\kappa_0}{\sqrt{(\gamma_0^2-1)}}[z-ct/\gamma_0]\sqrt{(1-\xi^2)}\right\}. \tag{35}$$

The integral in (35) may be evaluated (Prudnikov *et al.* 1986, eq. 2.12.21.6) to give finally

$$\psi_{\gamma_0,\beta}(\rho, z, t) = \exp\left(\frac{\mathrm{i}\beta\gamma_0[z-\gamma_0 ct]}{(\gamma_0^2-1)}\right)\frac{\sin\{\kappa_0\sqrt{[(\gamma_0^2/(\gamma_0^2-1))[z-ct/\gamma_0]^2+\rho^2]}\}}{\sqrt{[(\gamma_0^2/(\gamma_0^2-1))[z-ct/\gamma_0]^2+\rho^2]}}. \tag{36}$$

As $\gamma_0 > 1$, $\psi_{\gamma_0,\beta}$ in (36) represents a waveform whose envelope is travelling in the positive z direction with speed $c/\gamma_0 < c$; i.e. a subluminal pulse. We note that at the pulse centre ($z = ct/\gamma_0$) on the z axis ($\rho = 0$), $|\psi_{\gamma_0,\beta}|$ attains its maximum value of $\kappa_0 = \beta\gamma_0/\sqrt{(\gamma_0^2-1)}$. On the z axis the width of the 'main lobe' of $|\psi_{\gamma_0,\beta}|$ (the distance between which the argument of the sine function in (36) first takes on the value π) about the pulse centre $z = ct/\gamma_0$ is given by $2\pi(\gamma_0^2-1)/\beta\gamma_0^2 = 2\pi\beta/\kappa_0^2$. At the pulse centre the width of the 'main lobe', in the ρ direction, is given by $2\pi\sqrt{(\gamma_0^2-1)}/\beta\gamma_0 = 2\pi/\kappa_0$. Thus we see that greater localization is achieved for those HWE solutions in this family that have larger β values, or, for fixed β for those HWE solutions in families corresponding to values of γ_0 closer to one (i.e. the speed of the pulse approaches c).

In figures 11 and 12 we have shown normalized surface plots of $\mathrm{Re}\{\psi_{\gamma_0,\beta}(\boldsymbol{r}, t)\}$,

Figure 11

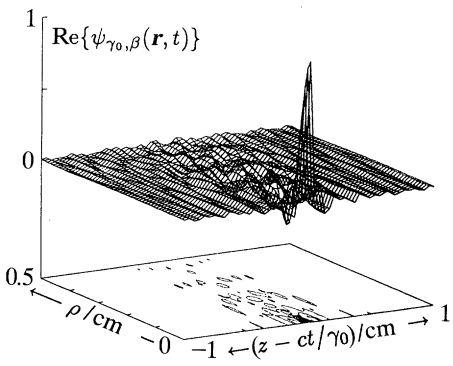

Figure 12

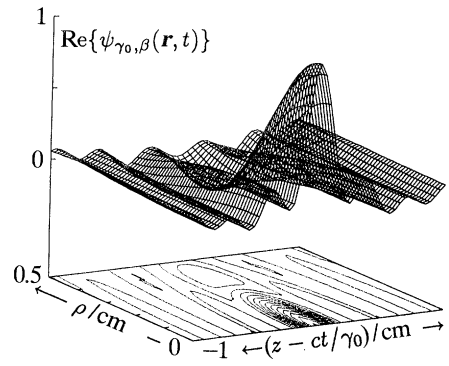

Figure 11. Normalized surface plot of the subluminal HWE solution pulse $\mathrm{Re}\{\psi_{\gamma_0,\beta}(\boldsymbol{r},t)\}$, where $\psi_{\gamma_0,\beta}$ is given in (36), for the values $t=0$, $\beta=50$, $|z-ct/\gamma_0|\leqslant 1$ cm, $0\leqslant\rho\leqslant 0.5$ cm, and $\gamma_0=2$. The pulse centre travels with speed $\frac{1}{2}c$.

Figure 12. Normalized surface plot of the subluminal HWE solution pulse $\mathrm{Re}\{\psi_{\gamma_0,\beta}(\boldsymbol{r},t)\}$, where $\psi_{\gamma_0,\beta}$ is given in (36), for the values $t=0$, $\beta=10$, $|z-ct/\gamma_0|\leqslant 1$ cm, $0\leqslant\rho\leqslant 0.5$ cm, and $\gamma_0=2$. The pulse centre travels with speed $\frac{1}{2}c$. Note the broadening of both the pulse waist and duration, as compared with figure 11.

where $\psi_{\gamma_0,\beta}$ is given in (36), for two different values of β. We see that a decrease in β results in a broadening of the pulse waist and duration.

4. Superpositions of LW solutions and finite energy conditions

The FWM and BG pulses, defined by (8) and (14), the constant speed family of superluminal pulses, defined by (29), and the constant speed family of subluminal pulses, defined by (36), are all HWE solutions for arbitrary choices of the positive real parameter β present in the solution. As such, a weighted superposition of members of each family of solutions, with respect to the parameter β,

$$\Theta(\boldsymbol{r},t)=\int_0^\infty \mathrm{d}\beta F(\beta)\,\psi_\beta(\boldsymbol{r},t), \tag{37}$$

will also have a HWE solution. In (37) $F(\beta)$ is an arbitrary 'spectrum', or weighting, and we have used the symbol ψ_β to denote an arbitrary member of one of the above mentioned HWE solution families.

The transform domain representations of the above luminal and superluminal HWE solution families (given, respectively, in (18), and (25)) share the property that they may be written in the form

$$\Psi_\beta(\kappa,k_z,\omega)=\Xi(\kappa,\beta)\,\delta[k_z-f_\kappa(\beta)]\,\delta[\omega-g_\kappa(\beta)], \tag{38}$$

where $f_\kappa(\beta)$ and $g_\kappa(\beta)$ are functions of κ and β such that $\kappa^2+f_\kappa^2(\beta)-g_k^2(b)/c^2=0$. The energy of the superposition (37) is given by

$$\mathscr{E}=\int_{\mathbb{R}^3}\mathrm{d}\boldsymbol{r}\,|\Theta(\boldsymbol{r},t)|^2. \tag{39}$$

In Appendix B we show how this energy expression may be rewritten as

$$\mathscr{E} = \frac{1}{(2\pi)^4}\int_0^\infty \mathrm{d}\beta\,|F(\beta)|^2 \int_0^\infty \mathrm{d}\kappa \frac{\kappa}{|\mathrm{d}f_\kappa(\beta)/\mathrm{d}\beta|}|\Xi(\kappa,\beta)|^2, \tag{40}$$

for a superposition $\Theta(\boldsymbol{r},t)$ of members of a family of HWE solutions whose transform domain representation is of the form (38). A straightforward modification of (40) gives the energy of superposition of the superluminal pulses, given through (33). Equation (40) is quite useful, as it obviates the need for manipulating the often cumbersome expression (39) on an *ad hoc* basis for any particular HWE solution family we choose. All we need do is substitute for the constraint $f_\kappa(\beta)$ and the weighting function $\Xi(\kappa,\beta)$. Using (40) we can obtain bounds for the superposition weighting, $F(\beta)$, in order that the superposition $\Theta(\boldsymbol{r},t)$ have finite total energy. This consideration is clearly important for launching approximate realisations of these superpositions from (necessarily) finite apertures.

In particular, for both LW and BG pulses, comparison of (38) with (6) shows that $f_\kappa(\beta) = \beta - \kappa^2/4\beta$. For LW pulses, where the weighting $\Xi(\kappa,\beta)$ is given in (7), the energy integral (40) becomes

$$\mathscr{E}|_{\mathrm{LW}} = \frac{1}{16}\int_0^\infty \mathrm{d}\beta\,|F(\beta)|^2 \int_0^\infty \mathrm{d}\kappa \frac{\kappa}{\kappa^2+4\beta^2}\exp(-\kappa^2 z_0/2\beta), \tag{41}$$

and using standard manipulations of the κ integral (Donnelly & Ziolkowski 1992) we obtain the inequality, previously given in (10), to be satisfied by the superposition spectrum F in (27). For the zero-order BG pulses, whose weight $\Xi(\kappa,\lambda,\beta)$ is given in (13), the energy integral (40) becomes

$$\mathscr{E}|_{\mathrm{BG}} = 4\pi^2 z_0 \int_0^\infty \mathrm{d}\beta\,|F(\beta)|^2 \int_0^\infty \mathrm{d}\kappa \frac{\kappa}{\kappa^2+4\beta^2}\left[I_0\left(\frac{\lambda z_0 \kappa}{2\beta}\right)\right]^2 \exp(-z_0[\lambda^2+\kappa^2]/2\beta), \tag{42}$$

or, if we make the change of variable $\kappa/\beta = \zeta$ in the inner integral,

$$\mathscr{E}|_{\mathrm{BG}} = 4\pi^2 z_0 \int_0^\infty \mathrm{d}\beta\,|F(\beta)|^2 \exp(-z_0\lambda^2/2\beta) \int_0^\infty \mathrm{d}\zeta \frac{\zeta[I_0(\frac{1}{2}\lambda z_0\zeta)]^2}{4+\zeta^2}\exp(-\tfrac{1}{2}z_0\beta\zeta^2). \tag{43}$$

A crude sufficient condition on the spectrum $F(\beta)$, so that $\mathscr{E}|_{\mathrm{BG}}$ remains finite, may be found. For $0 < z < 1$ we have $I_0(z) < 2$, while for $z > 1$, $I_0(z) < \mathrm{e}^z/\sqrt{(2\pi z)}$ (see (A 5)). If we denote the inner integral in (43) by D, we have the inequality

$$D < \int_0^{2/\lambda z_0} \mathrm{d}\zeta \frac{4\zeta}{4+\zeta^2}\exp(-\tfrac{1}{2}z_0\beta\zeta^2) + \frac{1}{\pi\lambda z_0}\int_{2/\lambda z_0}^\infty \mathrm{d}\zeta \frac{\exp(\lambda z_0\zeta)\exp(-\tfrac{1}{2}z_0 b\zeta^2)}{4+\zeta^2}. \tag{44}$$

A further inequality may be obtained by replacing the denominators of both integrands in (44) by 4, and extending the range of integration in the second integral to $-\infty$. With these alterations the integrals in (44) may be evaluated, and we have

$$\begin{aligned} D &< \frac{1-\exp(-2\beta/z_0\lambda^2)}{\beta z_0} + \frac{\exp(\lambda^2 z_0/2\beta)}{(2z_0)^{\frac{3}{2}}\lambda\sqrt{(\beta\pi)}} \\ &< \frac{1}{\beta z_0} + \frac{\exp(\lambda^2 z_0/2\beta)}{(2z_0)^{\frac{3}{2}}\lambda\sqrt{(\beta\pi)}}. \end{aligned} \tag{45}$$

Thus, a superposition, of the form (37), of zero-order BG pulses will have finite energy if we choose a spectrum F satisfying

$$\int_0^\infty \mathrm{d}\beta\,|F(\beta)|^2\left\{\frac{\exp(-z_0\lambda^2/2\beta)}{\beta z_0}+\frac{1}{(2z_0)^{\frac{3}{2}}\lambda\sqrt{(\pi\beta)}}\right\}<\infty. \tag{46}$$

For a superposition over the constant speed family of superluminal pulses, given in (29), we find, by comparison of (25) with (38), that

$$f_\kappa(\beta)=\gamma_0[-\beta+\sqrt{[\kappa^2(1-\gamma_0^2)+\gamma_0^2\beta^2]}]/(1-\gamma_0^2), \tag{47}$$

and the weighting $\Xi(\kappa,\beta)$ is given in (26). In this case the energy integral (40) becomes

$$\mathscr{E}=\frac{(2\pi)^2(1-\gamma_0^2)^{\frac{3}{2}}}{\gamma_0}\int_0^\infty \mathrm{d}\beta\,|F(\beta)|^2\int_0^\infty\frac{\mathrm{d}\kappa}{\kappa}\frac{\exp[-2\gamma_0 z_0\sqrt{(\kappa^2+\nu_0^2)}/\sqrt{(1-\gamma_0^2)}]}{\sqrt{(\kappa^2+\nu_0^2)}\,[\sqrt{(1-\gamma_0^2)}\,\sqrt{(\kappa^2+\nu_0^2)}-\gamma_0^2\beta]}, \tag{48}$$

where again $\nu_0^2=\gamma_0^2\beta^2/(1-\gamma_0^2)$. The integral with respect to κ in (48) does not converge. Hence, *no weighted superposition of superluminal pulses of the form* (29) *will have finite energy*. The problem comes from the $1/\kappa$ term in (48). Hence, considering the weighting $\Xi(\kappa,\gamma_0,\beta)$ in (26), if instead we chose as weighting, say,

$$\Xi(\kappa,\gamma_0,\beta)=\frac{(2\pi)^3}{\sqrt{\kappa}\,\sqrt{(\kappa^2+\nu_0^2)}}\exp[-z_0\gamma_0\sqrt{(\kappa^2+\nu_0^2)}/\sqrt{(1-\gamma_0^2)}], \tag{49}$$

the resulting space-time pulses would still be superluminal, and it would be possible to take weighted superpositions (with respect to β) of such pulses, such that the superposition had finite energy. Unfortunately, the choice of weighting (49) leads to space-time superluminal pulses that cannot be found in closed form. However, as the proposed weighting Ξ in (49) has a slower decay with increasing κ than does the original Ξ in (26), the uncertainty ideas explored in Appendix A lead us to conclude that our new family of superluminal pulses would possess better localization properties than do the previous ones.

5. Localized wave solutions of the Klein–Gordon equation

Consider the Klein–Gordon equation (KGE):

$$\left\{\frac{1}{c^2}\frac{\partial^2}{\partial t^2}-\nabla^2+\mu^2\right\}\psi(\boldsymbol{r},t)=0, \tag{50}$$

where $\mu>0$. Applying Fourier transforms to (50) gives

$$\{\kappa^2+k_z^2-(\omega/c)^2+\mu^2\}\,\mathscr{F}_{r,t}\{\psi\}(\boldsymbol{k},\omega)=0. \tag{51}$$

Following the analysis of the HWE, we realise that any rotationally invariant solution of the KGE will have a Fourier transform whose support lies on the surface

$$\kappa^2+k_z^2-(\omega/c)^2+\mu^2=0. \tag{52}$$

This surface is shown in figure 13. Once again, to consider Fourier transforms of KGE solutions whose supports are lines lying on the surface (52), we shall instead consider the projections of the support lines onto the $k_z,\omega/c$ plane.

Rather than catalogue various types of KGE solutions, as we did in the HWE case,

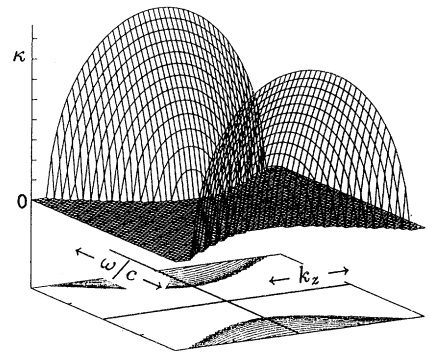

Figure 13. The surface $\kappa^2+k_z^2-(\omega/c)^2+\mu^2=0$, for the Klein–Gordon equation, is shown above the $k_z, \omega/c$ plane, and for the value $\mu=\frac{1}{2}$.

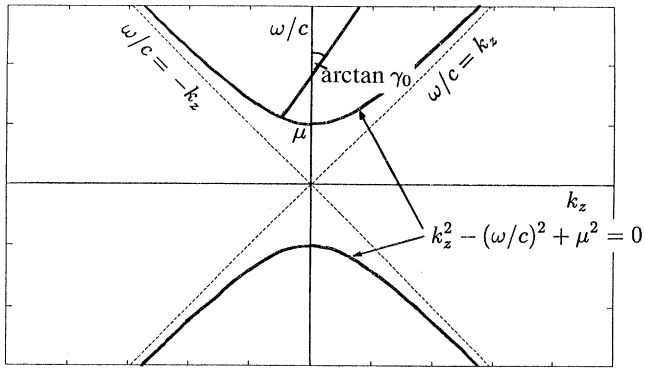

Figure 14. Projection of the support line of the transform of a member of a constant speed superluminal family of KGE solutions, for an arbitrary β value.

here we shall investigate families of superluminal and subluminal pulses. In figure 14 we have shown an arbitrary member of a family of straight projection lines, each having the same reciprocal slope γ_0 $(0<\gamma_0<1)$.

It is relatively straightforward to find the KGE solution line corresponding to this projection. This solution line will, correspond to a KGE solution whose Fourier transform is given by

$$\mathscr{F}_{r,t}\{\psi_{\gamma_0,\beta}\}(\kappa,k_z,\omega)=\Xi(\kappa,\gamma_0,\beta)\,\delta(k_z-\gamma_0[-\beta+\sqrt{[(\kappa^2+\mu^2)(1-\gamma_0^2)+\gamma_0^2\beta^2]}]/(1-\gamma_0^2))$$
$$\times\,\delta(\omega-c[-\beta\gamma_0^2+\sqrt{[(\kappa^2+\mu^2)(1-\gamma_0^2)+\gamma_0^2\beta^2]}]/(1-\gamma_0^2)), \quad (53)$$

where Ξ is an arbitrary weighting function to be associated with this solution line. This form is to be compared with the Fourier transform of the arbitrary HWE superluminal pulse, given in (25). If we now choose

$$\Xi(\kappa,\gamma_0,\beta)=(2\pi)^3\exp(-\chi_0\sqrt{(\nu_0^2+\kappa_2)})/\sqrt{(\nu_0^2+\kappa^2)}, \quad (54)$$

where $\nu_0^2=\beta^2\gamma_0^2/(1-\gamma_0^2)+\mu^2$, and χ_0 is an arbitrary positive parameter, the exact space-time form of the KGE solution given through (53) may be determined. Applying inverse spatial and temporal Fourier transforms to (53) gives, eventually,

$$\psi_{\gamma_0,\beta}(\rho,z,t)=\exp\left(\frac{-\mathrm{i}\beta\gamma_0[z-\gamma_0 ct]}{(1-\gamma_0^2)}\right)\nu_0\int_1^\infty \mathrm{d}\xi\exp(-[\chi_0-\mathrm{i}\sigma_0]\nu_0)\,\xi J_0(\rho\nu_0\sqrt{(\xi^2-1)}), \quad (55)$$

Figure 15

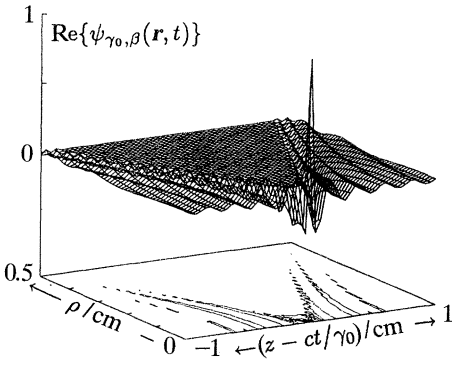

Figure 16

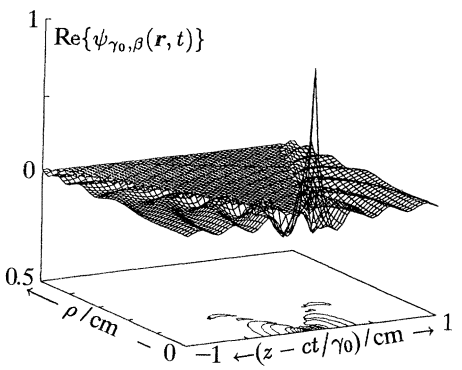

Figure 15. Normalized surface plot of the superluminal KGE solution pulse $\mathrm{Re}\{\psi_{\gamma_0,\beta}(\boldsymbol{r},t)\}$, where $\psi_{\gamma_0,\beta}$ is given in (57), for the values $t=0$, $\gamma_0=\frac{1}{2}$, $\beta=0.1$, $\mu=50$, $\chi_0=0.01$, $|z-ct/\gamma_0|\leqslant 1$ cm, and $0\leqslant\rho\leqslant 0.5$ cm.

Figure 16. Normalized surface plot of the superluminal KGE solution pulse $\mathrm{Re}\{\psi_{\gamma_0,\beta}(\boldsymbol{r},t)\}$, where $\psi_{\gamma_0,\beta}$ is given in (57), for the values $t=0$, $\gamma_0=\frac{1}{2}$, $\beta=100$, $\mu=50$, $\chi_0=0.01$, $|z-ct/\gamma_0|\leqslant 1$ cm, and $0\leqslant\rho\leqslant 0.5$ cm. Note the broadening of the pulse duration, and the different oscillatory behaviour of the solution inside the 'Mach cone', as compared with figure 15.

where we use σ_0 defined by

$$\sigma_0=(\gamma_0/\sqrt{(1-\gamma_0^2)})\,[z-ct/\gamma_0]. \tag{56}$$

The integral in (55) may be evaluated (Gradshteyn & Ryzhik 1980, eq. 6.646.1) to give

$$\psi_{\gamma_0,\beta}(\rho,z,t)=\exp\left(-\mathrm{i}\beta\gamma_0[z-\gamma_0 ct]/(1-\gamma_0^2)\right)\times\exp\{-\nu_0\sqrt{[(\chi_0-\mathrm{i}\sigma_0)^2+\rho^2]}\}/\sqrt{[(\chi_0-\mathrm{i}\sigma_0)^2+\rho^2]}. \tag{57}$$

The KGE solution given by (57) clearly represents a superluminal pulse ($0<\gamma_0<1$). In figures 15–18 we have shown normalized surface plots of the superluminal KGE solution pulse $\mathrm{Re}\{\psi_{\gamma_0,\beta}(\boldsymbol{r},t)\}$, where $\psi_{\gamma_0,t}$ is given in (57), for varying β, μ (i.e. mass term), and χ_0.

We see that as μ is decreased, the oscillatory behaviour of the solution within the 'Mach cone' becomes difficult to detect (relative to the amplitude at the pulse centre). Also, decreasing the value of χ_0 causes a decrease in the change of the solution across the Mach cone.

It should also be noted that had we chosen projections of KGE solution lines that had reciprocal slope one ($\gamma_0=1$), instead of (53) we should arrive at a KGE solution whose Fourier transform is given by

$$\mathscr{F}_{r,t}\{\psi_{\gamma_0,\beta}\}(\kappa,k_z,\omega)=\Xi(\kappa,\beta)\,\delta(k_z-(\kappa^2+(\mu^2-\beta^2))/2\beta)\,\delta(\omega-c[\kappa^2+(\mu^2+\beta^2)]/2\beta). \tag{58}$$

If we now choose

$$\Xi(\kappa,\beta)=((2\pi)^2/\beta)\exp\left(-z_0\kappa^2/2\beta\right), \tag{59}$$

where $z_0>0$ is arbitrary, then the exact space-time form of the KGE solution given through (58) is given by

$$\psi_\beta(\rho,z,t)=\frac{1}{\beta}\exp\left(\mathrm{i}z(\mu^2-\beta^2)/2\beta\right)\exp\left(-\mathrm{i}tc(\mu^2+\beta^2)/2\beta\right)\int_0^\infty \mathrm{d}\kappa\,\kappa J_0(\kappa\rho)\times\exp\left[-\kappa^2[z_0-\mathrm{i}(z-ct)]/2\beta\right]. \tag{60}$$

Figure 17

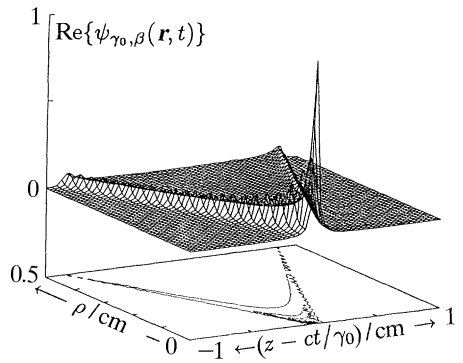

Figure 18

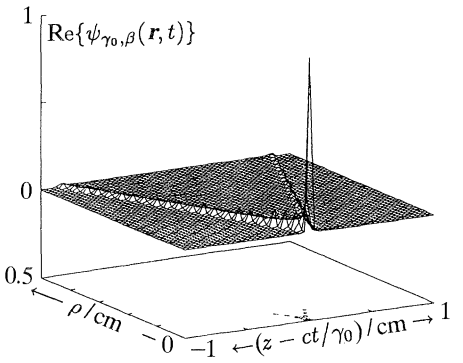

Figure 17. Normalized surface plot of the superluminal KGE solution pulse $\mathrm{Re}\{\psi_{\gamma_0,\beta}(\boldsymbol{r},t)\}$, where $\psi_{\gamma_0,\beta}$ is given in (57), for the values $t=0$, $\gamma_0=\frac{1}{2}$, $\beta=0.1$, $\mu=1$, $\chi_0=0.01$, $|z-ct/\gamma_0|\leqslant 1$ cm, and $0\leqslant\rho\leqslant 0.5$ cm. Note that the mass term is lower than in figure 15 and, the oscillatory behaviour inside the 'Mach cone' is undetectable.

Figure 18. Normalized surface plot of the superluminal KGE solution pulse $\mathrm{Re}\{\psi_{\gamma_0,\beta}(\boldsymbol{r},t)\}$, where $\psi_{\gamma_0,\beta}$ is given in (57), for the values $t=0$, $\gamma_0=\frac{1}{2}$, $\beta=0.1$, $\mu=50$, $\chi_0=0.002$, $|z-ct/\gamma_0|\leqslant 1$ cm, and $0\leqslant\rho\leqslant 0.5$ cm. Again, oscillatory behaviour inside the 'Mach cone' is undetectable, and, moreover, the change in the pulse when crossing the Mach cone is smaller (relative to the pulse centre amplitude) then in figure 17. The serrations of the surface along the Mach cone are an artefact due to plotting grid coarseness.

The integral in (60) may be evaluated (Gradshteyn & Ryzhik 1980, eq. 6.631.4) to give

$$\psi_\beta(\rho,z,t)=\exp(\mathrm{i}z(\mu^2-\beta^2)/2\beta)\exp(-\mathrm{i}tc(\mu^2+\beta^2)/2\beta)\times\exp(-\rho^2\beta/2[z_0-\mathrm{i}(z-ct)])/[z_0-\mathrm{i}(z-ct)]. \quad (61)$$

The KGE solution in (61) is essentially the same type of LWE KGE solution found previously by us (Donnelly & Ziolkowski 1992). Comparing it with the HWE FWM solution, given in (8), we see that ψ_β in (61) has essentially the same localization properties as that LW solution, but is travelling at luminal speed.

On the other hand, if one proceeds with a projection analogous to the HWE result shown in figure 10, one obtains the Fourier transform

$$\begin{aligned}\mathscr{F}_{r,t}\{\psi_{\gamma_0,\beta}\}(\boldsymbol{r},t)=\;&\Xi_1(\kappa,\gamma_0,\beta)\,\delta(k_z-\gamma_0[\beta+\sqrt{[\beta^2\gamma_0^2-(\kappa^2+\mu^2)(\gamma_0^2-1)]}]/(\gamma_0^2-1))\\&\times\delta(\omega-c[\beta\gamma_0^2+\sqrt{[\gamma_0^2\beta^2-(\kappa^2+\mu^2)(\gamma_0^2-1)]}]/(\gamma_0^2-1))\\&+\Xi_2(\kappa,\gamma_0,\beta)\,\delta(k_z-\gamma_0[\beta-\sqrt{[\beta^2\gamma_0^2-(\kappa^2+\mu^2)(\gamma_0^2-1)]}]/(\gamma_0^2-1))\\&\times\delta(\omega-c[\beta\gamma_0^2-\sqrt{[\beta^2\gamma_0^2-(\kappa^2+\mu^2)(\gamma_0^2-1)]}]/(\gamma_0^2-1)),\end{aligned} \quad (62)$$

where κ now lies in the range $0\leqslant\kappa\leqslant[(\beta\gamma_0/\sqrt{(\gamma_0^2-1)})^2-\mu^2]^{\frac{1}{2}}\equiv\kappa_0$. If we choose the same weighting functions Ξ_1 and Ξ_2 defined by (34):

$$\Xi_1(\kappa,\gamma_0,\beta)\equiv\Xi_2(\kappa,\gamma_0,\beta)=(2\pi)^3/2\sqrt{(\kappa_0^2-\kappa^2)}, \quad (63)$$

then the exact space-time form of the HWE solution defined by (62) may be determined by proceeding exactly as we did in §3*f*. This process yields the KGE solution

$$\psi_{\gamma_0,\beta}(\rho,z,t)=\exp\left(\frac{\mathrm{i}\beta\gamma_0[z-\gamma_0 ct]}{(\gamma_0^2-1)}\right)\frac{\sin\{\kappa_0\sqrt{((\gamma_0^2/(\gamma_0^2-1))[z-ct/\gamma_0]^2+\rho^2)}\}}{\sqrt{((\gamma_0^2/(\gamma_0^2-1))[z-ct/\gamma_0]^2+\rho^2}}). \quad (65)$$

As $\gamma_0 > 1$, $\psi_{\gamma_0,\beta,\mu}$ in (65) represents a waveform whose envelope is travelling in the positive z direction with speed $v_g = c/\gamma_0 < c$; i.e. a subluminal pulse. This result recovers the unidirectional KGE solution reported by Ziolkowski *et al.* (1991).

Aside from the actual definition of κ_0, we note that the subluminal KGE solution (65) is identical to the subluminal HWE solution (36). Introducing the standard relativistic factor $\gamma_{\text{rel}}^2 = [1-(v_g/c)^2]^{-\frac{1}{2}}$, we can write $\gamma_0^2/(\gamma_0^2-1) = \gamma_{\text{rel}}^2$ and specify the terms

$$k_z(\kappa_0) = \beta\gamma_0/(\gamma_0^2-1) = \gamma_{\text{rel}}^2(v_g/c)\,\beta, \tag{66a}$$

$$\omega(\kappa_0)/c = [\kappa_0^2+k_z^2+\mu^2]^{\frac{1}{2}} = \gamma_{\text{rel}}^2\,\beta, \tag{66b}$$

$$\kappa_0 = (\beta^2\gamma_{\text{rel}}^2-\mu^2)^{\frac{1}{2}}, \tag{66c}$$

$$v_p = \omega(\kappa_0)/k_z = c\gamma_0 = c^2/v_g, \tag{66d}$$

so that we rewrite (65) as

$$\psi_{\gamma_0,\beta}(\rho,z,t) = \exp(ik_z(z-v_p\,t))\,\frac{\sin[\kappa_0\sqrt{[\rho^2+\gamma_{\text{rel}}^2(z-v_g\,t)^2]}]}{\sqrt{[\rho^2+\gamma_{\text{rel}}^2(z-v_g\,t)^2]}}. \tag{67}$$

The parameter β is still free, the propagation constants v_g, κ_0, k_z, and ω following from (66). We could thus continue with our analysis by taking superpositions of (67) over this free parameter β to obtain finite energy solutions. Another choice would be to fix v_g and then form superpositions over the angular frequency ω since (66b) gives $\beta = \omega/(\gamma_{\text{rel}}^2\,c)$. This would yield a localized finite energy solution travelling along z at speed v_g.

A similar form for (36) can also be obtained simply by taking $\mu \to 0$ in the frequency, wavenumber, and phase velocity expressions given in (66); finite energy superpositions, as discussed in §4, would then be available for the HWE. However, without labouring any further into finite energy superpositions, we can note several interesting features shared by the subluminal KGE and HWE results. As noted above, the subluminal HWE (36) and KGE (67) solutions differ only by their values for the propagation constants. None the less, we now will interpret (67) as a representation of a massive, spinless particle travelling with speed v_g along the z-axis and the corresponding HWE result (36) as a localized packet of waves. The dispersion relation (52) then represents the energy of the particle if we define the energy $E = \hbar w$ and the momentum $p^2 = \hbar^2(\kappa^2+k_z^2)$. Similarly, the dispersion relation (12) represents the wave energy if we introduce the same energy and momentum definitions. We note that both the KGE $|\psi_{\gamma_0,\beta,\mu}|$ and the HWE $|\psi_{\gamma_0,\beta}|$ solutions attain their maximum value of κ_0 at their centres ($z = ct/\gamma_0 = v_g\,t$) on the z-axis ($\rho = 0$) and that the weights given by (34) and (63) could be adjusted by $1/\kappa_0$ to yield unity normalizations of these solutions instead. On the z-axis the width of the 'particle' and 'localized wave packet' about their centres at $z = ct/\gamma_0 = v_g\,t$ is given by

$$2\pi[(\gamma_0^2-1)/\kappa_0^2\,\gamma_0^2]^{\frac{1}{2}} = 2\pi/(\gamma_{\text{rel}}\,\kappa_0).$$

This longitudinal extent decreases as the particle or wave speed increases towards c and the relativistic factor γ_{rel} increases. The transverse width of the 'particle' and 'localized wave packet' about their centres in the ρ direction, is given simply by $2\pi/\kappa_0$. As one would expect from relativistic considerations, the transverse waist is not explicitly dependent on the factor γ_{rel}. Thus we see that greater localization of the particle or the localized wave packet is achieved for those cases having larger β, hence, κ_0 values, or, for fixed β, those cases corresponding to values of γ_0 closer to one (i.e. as the group and phase speeds of the particle or the localized wave packet

Figure 19

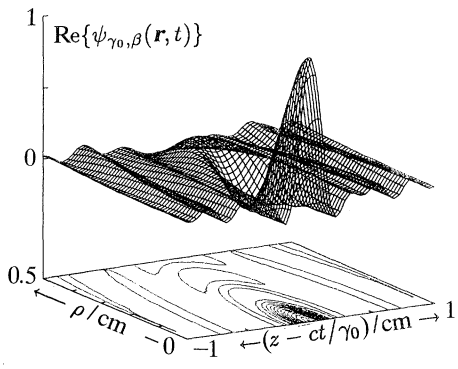

Figure 20

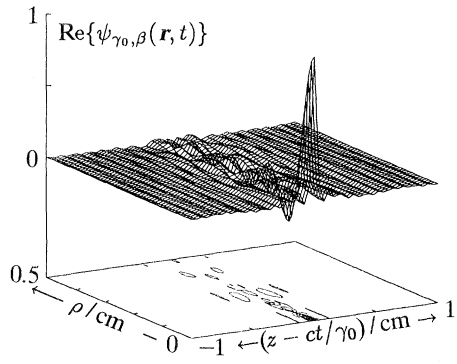

Figure 19. Normalized surface plot for the subluminal KGE solution pulse $\mathrm{Re}\{\psi_{\gamma_0,\beta}(\boldsymbol{r},t)\}$, where $\psi_{\gamma_0,\beta}$ is given in (65), for the values $\mu = 1$, $t = 0$, $\beta = 20$, $|z - ct/\gamma_0| \leqslant 1$ cm, $0 \leqslant \rho \leqslant 0.5$ cm, and $\gamma_0 = 5$ (so that the pulse centre travels with speed $\frac{1}{5}c$.

Figure 20. Normalized surface plot for the subluminal KGE solution pulse $\mathrm{Re}\{\psi_{\gamma_0,\beta}(\boldsymbol{r},t)\}$, where $\psi_{\gamma_0,\beta}$ is given in (65), for the values $\mu = 1$, $t = 0$, $\beta = 20$, $|z - ct/\gamma_0| \leqslant 1$ cm, $0 \leqslant \rho \leqslant 0.5$ cm, and now $\gamma_0 = 1.1$ (so that the pulse centre travels with speed $c/1.1$). In comparison with the pulse shown in figure 19, the pulse here has the same mass but increased kinetic energy: the pulse here is more highly localized.

approach c). However, we must remember that the exact values for these parameters are obtained differently between the KGE and the HWE solution families. For instance, a decrease in either μ or γ_0 leads to an increase of κ_0, which in turn results in a narrowing of the particle's transverse waist and longitudinal extent. On the other hand, one can only either increase the value of β or decrease γ_0 so as to increase κ_0 and thus produce a similar effect on the properties of the localized wave packet.

In figures 19 and 20 we show a normalized surface plot of $\mathrm{Re}\{\psi_{\gamma_0,\beta}(\boldsymbol{r},t)\}$, where the KGE solution $\psi_{\gamma_0,\beta}$ is given by (65). Comparing figures 19 and 20 we find that keeping the mass term $[\mu]$ and β constant, while increasing the speed (hence kinetic energy) of the pulse, results in an increase in the value of κ_0, hence an increase in the pulse localization.

We note that there have been many connections between particle and purely wave solutions, generally based on standing waves or plane waves. The relationships between (36) and (67) provide a direct connection between *localized* massless (HWE) and massive (KGE) solutions. We note that there are some properties directly shared between the subluminal (or superluminal) HWE or KGE solutions without specifying any case dependent parameters. For example, the phase and group speeds in both instances must strictly satisfy the relation:

$$v_{\mathrm{p}}\, v_{\mathrm{g}} \equiv c^2. \tag{68}$$

This property can be seen to be intimately connected to the subluminal (or superluminal) nature of these solutions and their free space dispersion relations. It is a natural generalization of the luminal solution property that $v_{\mathrm{p}} = v_{\mathrm{g}} = c$.

6. Discussion

In this paper we have made transparent our previous 'algebraic' method for obtaining interesting, non-separable, localized solutions of constant coefficient

homogeneous linear partial differential equations. Considering the HWE, we dealt with solutions whose Fourier transforms have supports along lines lying on the surface $\kappa^2 + k_z^2 - (\omega/c)^2 = 0$ in phase space. We further note that these supports would equally well have been taken as patches or points, although these choices were not considered explicitly. Varying the free parameter (present in most of the solutions considered) caused the corresponding support line to sweep out a subset of that phase space surface and, hence, caused the projection of the support line to sweep out some region of the k_z, ω/c plane lying within the wedges $-\omega/c \leqslant k_z \leqslant \omega/c$ (e.g. see figure 2).

The process of designing a family of non-separable, localized HWE solutions can thus begin by choosing a one parameter family of straight lines that sweeps out some region of the mentioned k_z, ω/c-plane wedges. The corresponding family of transformed solution supports is readily found. The coupling of κ, k_z, and ω on any support line is what causes the corresponding space-time solutions to be non-separable. The degree of localization of the solution (about the propagation axis) is controlled by the weighting associated with the transformed solution support line; in particular, by effectively treating κ as a free parameter, one can create an appropriately designed weighting over the variable κ to produce the desired localization in the space-time domain. Considering, for example, a support line on which $\kappa \to \infty$, we obviously require the weighting to be such that the inverse Fourier transform exists; but beyond this requirement, we observe that tempering the decay of the weighting (as $\kappa \to \infty$) will, in general, cause a greater degree of localization (in accordance with satisfaction of the 'uncertainty relation' (16)).

We demonstrated that by choosing the projections of the support lines to have slopes greater than (respectively, less than) one, in the k_z, ω/c plane, one can obtain solutions whose envelopes (localized component) travelled with speed greater than (respectively, less than) c; i.e. superluminal (subluminal) solutions. Moreover, the examples we presented included a certain degree of localization as well. Identical forms were obtained for the subluminal localized wave HWE and KGE solutions, which led to a direct connection between the corresponding localized wave packet and particle interpretations of those solutions. Common properties of those subluminal solutions were identified such as an increase in the degree of localization as their energy increased (mass remaining constant for the KGE pulse); and it was shown that those solutions require a specific relationship between their phase and group speeds: $v_g v_p = c^2$, which is a generalization of the usual luminal values $v_g = v_p = c$.

It is important to realize that the various weightings associated with the support lines that we considered here were chosen *solely* to guarantee that a closed form space-time solution could be found (i.e. that the inverse Fourier transform could be evaluated in closed form). To more fully exploit this design procedure for purposes of launching, say, acoustic realizations of (approximations to) localized waves and their superpositions from an array of transducers (see Donnelly & Ziolkowski (1992) for a summary of experiments), one would choose a support line weighting that gave the desired localization properties, and then numerically invert the Fourier transform. One would then obtain the requisite time domain signals to be fed into a transducer array to reproduce the solution, at least in the near field of the array.

In addition, it must be noted that in this paper we chose particular solution families whose Fourier transforms have supports which projected onto a family of straight lines in the k_z, ω/c plane. This is not necessary. We could, for example, have

chosen a one parameter family of hyperbolae that 'spanned' either wedge in the HWE case (shown in figure 2), or the interiors of either hyperbola in the KGE case (shown in figure 14). These considerations lead us to pose the following question: what is, *a priori*, the speed of the envelope of the HWE solution corresponding to an arbitrary support line projection in the k_z, ω/c plane (i.e. to an arbitrary support line)? Linked to this question is the important notion of the group velocity of a pulse. The localized waves we have considered are broadband either temporally or spatially or both. Most considerations of group velocity deal with narrow band (in frequency) wave packets, and the concepts used in that case often break down when extended to broadband signals (Jackson 1975). In this context the idea of group velocity seems important, albeit ambiguous, and will be addressed in a future publication.

This work was done when R.D. was a Visiting Scholar in the Department of Electrical and Computer Engineering at the University of Arizona, during the autumn of 1991. This work was supported by the Canadian Natural Sciences and Engineering Research Council Operating Grant OGPIN 011.

Appendix A. The uncertainty relation for localized waves and Bessel–Gauss pulses

Here we shall make more precise statements made in the main body of the paper concerning the inequality

$$W \times B \equiv \frac{\int_{\mathbb{R}^2} \mathrm{d}x\,\mathrm{d}y\,\rho^2 |\psi(\rho,z,t)|^2}{\int_{\mathbb{R}^2} \mathrm{d}x\,\mathrm{d}y\,|\psi(\rho,z,t)|^2} \times \frac{\int_{\mathbb{R}^2} \mathrm{d}k_x\,\mathrm{d}k_y\,\kappa^2 |\mathscr{F}_{x,y}\{\psi\}(\kappa,z,t)|^2}{\int_{\mathbb{R}^2} \mathrm{d}k_x\,\mathrm{d}k_y |\mathscr{F}_{x,y}\{\psi\}(\kappa,z,t)|^2} \geqslant \frac{1}{2}, \tag{A 1}$$

as it pertains to the FWM and zero-order BG pulses. In (A 1) we have used the symbols W and B to denote the (transverse to propagation axis) 'waist' and (corresponding transform domain) 'spatial bandwidth' defined there.

The Ziolkowski LW pulses, ψ_{FWM}, are given in (8), and their full space-time Fourier transforms through (6) and (7). The expression $|\mathscr{F}_{x,y}\{\psi_{\mathrm{FWM}}\}(\kappa,z,t)|$ required for the bandwidth (B) quotient, is given equivalently by the magnitude of the inverse z and t Fourier transforms of (6). The delta functions in (6) contribute terms whose magnitudes are one, and so

$$\mathscr{F}_{x,y}\{\psi_{\mathrm{FWM}}\}(\kappa,z,t)| = |\Xi_{\mathrm{FWM}}(\kappa,\beta)| = \pi^2 \exp(-\kappa^2 z_0/4\beta).$$

The integrals in the expressions for W and B are readily evaluated, and we obtain

$$(W \times B)_{\mathrm{FWM}} = (z_0^2 + (z-ct)^2)/2\beta z_0 \times 2\beta/z_0. \tag{A 2}$$

From (A 2) we see that the waist of the FWM pulse changes as $z-ct$ changes, and that the bandwidth remains constant. We also see that the smallest value of the waist-bandwidth product is one, and this occurs at the pulse centre, $z = ct$, whereas the waist takes its smallest value, $z_0/2\beta$.

For the Overfelt zero-order BG pulses the analysis is not so simple. Here we have $\psi_{\mathrm{BG},0}$ as given in (14), and again we have

$$|\mathscr{F}_{x,y}\{\psi_{\mathrm{BG},0}\}(\kappa,z,t)| = |\Xi_{\mathrm{BG},0}(\kappa,\lambda,\beta)|.$$

The expressions for the waist and bandwidth here reduce to

$$W = \frac{\int_0^\infty \mathrm{d}\rho\, \rho^3 \left| J_0\left(\frac{\lambda z_0 \rho}{z_0 + \mathrm{i}(z-ct)}\right)\right|^2 \exp\left[-2\beta z_0 \rho^2/[z_0^2 + (z-ct)^2]\right]}{\int_0^\infty \mathrm{d}\rho\, \rho \left| J_0\left(\frac{\lambda z_0 \rho}{z_0 + \mathrm{i}(z-ct)}\right)\right|^2 \exp\left[-2\beta z_0 \rho^2/[z_0^2 + (z-ct)^2]\right]}, \tag{A 3}$$

$$B = \frac{\int_0^\infty \mathrm{d}\kappa\, \kappa^3 \left| I_0\left(\frac{\lambda z_0 \kappa}{2\beta}\right)\right|^2 \exp\left(-z_0 \kappa^2/2\beta\right)}{\int_0^\infty \mathrm{d}\kappa\, \kappa \left| I_0\left(\frac{\lambda z_0 \kappa}{2\beta}\right)\right|^2 \exp\left(-z_0 \kappa^2/2\beta\right)}. \tag{A 4}$$

To obtain an approximate expression for the product $(W \times B)_{\mathrm{BG},0}$ we shall assume that $\lambda \gg \beta > 0$. Note that this assumption is justified for the following reasons:

(i) It is known (Overfelt 1991) that the zero-order BG pulse reduces to the FWM pulse as $\lambda \to 0$, and so any 'improvement' of localization properties of the BG pulses can be expected to come from values of λ away from zero.

(ii) It is known (Ziolkowski 1985, 1989) that the FWM pulses possess little localization for small β.

Numerical studies of the integrands in (A 3) and (A 4) suggest that the following approximations are valid for λ only two or three times greater than β.

With the above assumptions then, we approximate I_0 and J_0 by the first terms of their asymptotic expansions (Abramowitz & Stegun 1965, eqs 9.2.1, 9.7.1)

$$I_0(\zeta) \sim \mathrm{e}^\zeta/\sqrt{(2\pi\zeta)}, \quad J_0(\zeta) \sim \sqrt{(2/\pi\zeta)}\cos\left(\zeta - \tfrac{1}{4}\pi\right). \tag{A 5}$$

With these approximations our expressions (A 3) and (A 4) for the waist and bandwidth of the zero-order BG pulse reduce to

$$W \approx \frac{\int_0^\infty \mathrm{d}\rho\, \rho^2 \{\cosh\left[\lambda\alpha\rho(z-ct)\right] + \sin\left[\lambda\alpha\rho z_0\right]\} \mathrm{e}^{-\beta\alpha\rho^2}}{\int_0^\infty \mathrm{d}\rho\, \{\cosh\left[\lambda\alpha\rho(z-ct)\right] + \sin\left[\lambda\alpha\rho z_0\right]\} \mathrm{e}^{-\beta\alpha\rho^2}}, \tag{A 6}$$

$$B \approx \frac{\int_0^\infty \mathrm{d}\kappa\, \kappa^2 \exp\left(-z_0(\kappa-\lambda)^2/2\beta\right)}{\int_0^\infty \mathrm{d}\kappa \exp\left(-z_0(\kappa-\lambda)^2/2\beta\right)}, \tag{A 7}$$

where $\alpha = 2z_0/[z_0^2 + (z-ct)^2]$. Two further approximations are justified by our assumptions. Since $\lambda \gg \beta$, the oscillations due to the $\sin\left[\lambda\alpha\rho z_0\right]$ terms in the waist expressions will cause the integrals involving these terms to contribute very little to both the numerator and denominator; we shall neglect their contribution. Additionally, we shall extend both ranges of integration to $-\infty$ in the expression (A 7) for the bandwidth. With these approximations, the integrals in the waist expression are known (Gradshteyn & Ryhzik 1980, eq. 3.546.2) and those in the bandwidth expression are easily evaluated. We arrive at

$$(W \times B)_{\mathrm{BG},0} \approx (1/4\beta)\{(z_0^2 + (z-ct)^2)/z_0 + \lambda^2(z-ct)^2\} \times \{\beta/z_0 + \lambda^2\}. \tag{A 8}$$

Considering (A 8), we see that the waist of the zero-order BG pulse varies with $z-ct$, whereas the bandwidth remains constant. This is so, in fact, regardless of our assumptions. The smallest value of the waist is $z_0/4\beta$, at the pulse centre, $z = ct$.

Considering the waist-bandwidth product for the FWM pulses, (A 2), and for the zero-order BG pulses, (A 8), we realize the following. The smallest value of the waist of the zero-order BG pulse (if $\lambda \gg \beta > 0$) is half that of the FWM pulse. Both waists/bandwidths decrease/increase as β increases. With the assumptions made, the value of λ does not affect the smallest value of the zero-order BG pulse waist, and moreover it seems to increase the waist of the pulse as it increases, for $z \neq ct$.

Appendix B. Derivation of energy expression (40)

The energy over a superposition of HWE solutions is given by (39), which we duplicate here for convenience, and rewrite using Parseval's theorem:

$$\mathscr{E} = \int_{\mathbb{R}^3} \mathrm{d}\boldsymbol{r}\, |\Theta(\boldsymbol{r}, t)|^2 \equiv \frac{1}{(2\pi)^3} \int_{R^3} \mathrm{d}\boldsymbol{k}\, |\mathscr{F}_{\boldsymbol{r}}\{\Theta\}(\boldsymbol{k}, t)|^2. \tag{B 1}$$

The HWE solution $\Theta(\boldsymbol{r}, t)$ is given as a superposition of the HWE superposition family $\psi_\beta(\boldsymbol{r}, t)$ (through (37)), where the transform domain form of $\psi_\beta(\boldsymbol{r}, t)$ is given in (38). Using (37) and (38) we may write

$$\begin{aligned} \mathscr{F}_{\boldsymbol{r}}(\Theta)(\boldsymbol{k}, t) &= \int_0^\infty \mathrm{d}\beta\, F(\beta)\, \mathscr{F}_t^{-1}\{\Psi_\beta\}(\boldsymbol{k}, t) \\ &= \frac{1}{2\pi} \int_0^\infty \mathrm{d}\beta\, F(\beta)\, \Xi(\kappa, \beta)\, \delta[k_z - f_\kappa(\beta)] \exp(-\mathrm{i}t g_\kappa(\beta)), \end{aligned} \tag{B 2}$$

where $\mathscr{F}_t^{-1}$ denotes the inverse temporal Fourier transform operator.

In equation (B 2) let us make the change of variable $f_\kappa(\beta) = \xi$, and assume that we can invert this relationship to obtain $\beta = f_\kappa^{-1}(\xi)$ (if f_κ, whose domain is $[0, \infty)$, is not a bijective mapping onto its range, then this argument may be modified). We then obtain

$$\begin{aligned} \mathscr{F}_{\boldsymbol{r}}\{\Theta\}(\boldsymbol{k}, t) &= \frac{1}{2\pi} \int_{f_\kappa(0)}^{f_\kappa(\infty)} \mathrm{d}\xi \frac{\mathrm{d}f_\kappa^{-1}(\xi)}{\mathrm{d}\xi} F(f_\kappa^{-1}(\xi))\, \Xi(\kappa, f_\kappa^{-1}(\xi))\, \delta(k_z - \xi) \exp(-\mathrm{i}t g_\kappa(f_\kappa^{-1}(\xi))) \\ &= \frac{A}{2\pi} \frac{\mathrm{d}f_\kappa^{-1}(k_z)}{\mathrm{d}k_z} F(f_\kappa^{-1}(k_z))\, \Xi(\kappa, f_\kappa^{-1}(k_z)) \exp(-\mathrm{i}t g_\kappa(f_\kappa^{-1}(\kappa_z))), \end{aligned} \tag{B 3}$$

where we assume that $k_{z_1} \equiv \min(f_\kappa(0), f_\kappa(\infty)) < k_z < \max(f_\kappa(0), f_\kappa(\infty)) \equiv k_{z_2}$, and the constant $A = \pm 1$ depending on whether $f_\kappa(\infty) \gtrless f_\kappa(0)$. Then (B 1) becomes

$$\mathscr{E} = \frac{1}{(2\pi)^5} \int_{\mathbb{R}^2} \mathrm{d}k_x\, \mathrm{d}k_y \int_{k_{z_1}}^{k_{z_2}} \mathrm{d}k_z \left| \frac{\mathrm{d}f_\kappa^{-1}(k_z)}{\mathrm{d}k_z} F(f_\kappa^{-1}(k_z))\, \Xi(\kappa, f_\kappa^{-1}(k_z)) \right|^2. \tag{B 4}$$

Making the 'inverse' change of variable $f_\kappa^{-1} = \beta$, so that $k_z = f_\kappa(\beta)$, our energy expression becomes

$$\mathscr{E} = \frac{1}{(2\pi)^4} \int_0^\infty \mathrm{d}\kappa\, \kappa \int_0^\infty \mathrm{d}\beta \left| \frac{\mathrm{d}f_\kappa^{-1}}{\mathrm{d}k_z}(k_z)|_{k_z = f_\kappa(\beta)} \right| |F(\beta)\, \Xi(\kappa, \beta)|^2. \tag{B 5}$$

It is readily demonstrated that

$$\frac{\mathrm{d}f_\kappa^{-1}}{\mathrm{d}k_z}(k_z)|_{k_z = f_\kappa(\beta)} \equiv \frac{1}{\mathrm{d}f_\kappa(\beta)/\mathrm{d}\beta}, \tag{B 6}$$

and so our energy expression becomes

$$\mathscr{E} = \frac{1}{(2\pi)^4}\int_0^\infty \mathrm{d}\beta\,|F(\beta)|^2 \int_0^\infty \mathrm{d}\kappa \frac{\kappa}{|\mathrm{d}f_\kappa(\beta)/\mathrm{d}\beta|}|\Xi(\kappa,\beta)|^2, \tag{B 7}$$

as was stated in (40) in the main text.

References

Abramowitz, M. & Stegun, I. 1965 *Handbook of mathematical functions*. New York: Dover.

Donnelly, R. & Ziolkowski, R. W. 1992 A method for constructing solutions of homogeneous partial differential equations: localized waves. *Proc. R. Soc. Lond.* A **437**, 673–692.

Gradshteyn, I. S. & Ryzhik, I. M. 1980 *Table of integrals, series, and products*. San Francisco: Academic Press.

Overfelt, P. L. 1991 Bessel–Gauss pulses. *Phys. Rev.* A **44**, 3941.

Prudnikov, A. P. *et al.* 1986 *Integrals and series*, vol. 2. New York: Gordon and Breach.

Ziolkowski, R. W. 1985 Exact solutions of the wave equation with complex source locations. *J. math. Phys.* **26**, 861.

Ziolkowski, R. W. 1989 Localized transmission of electromagnetic energy. *Phys. Rev.* A **39**, 2005.

Ziolkowski, R. W., Besieris, I. M. & Shaarawi, A. M. 1991 Localized wave representations of acoustic and electromagnetic radiation. *Proc. IEEE* **79**, 1371.

Ziolkowski, R. W., Besieris, I. M. & Shaarawi, A. M. 1993 Aperture realizations of exact solutions to homogeneous wave equations. *J. opt. Soc. Am.* A **10**, 75–87.

Received 14 May 1992; accepted 31 July 1992